SJSU SAN JOSÉ STATE UNIVERSITY

MTI MINETA TRANSPORTATION INSTITUTE

Experimental Investigations of Wind Shear from Passing a Vehicle

Hamid Rahai, PhD Jeremy Bonifacio, PhD
Assma Begum Ryan Moffit

CSUTC California State University Transportation Consortium

CALIFORNIA STATE UNIVERSITY LONG BEACH

CSU TRANSPORTATION CONSORTIUM

transweb.sjsu.edu/csutc

MINETA TRANSPORTATION INSTITUTE

Founded in 1991, the Mineta Transportation Institute (MTI), an organized research and training unit in partnership with the Lucas College and Graduate School of Business at San José State University (SJSU), increases mobility for all by improving the safety, efficiency, accessibility, and convenience of our nation's transportation system. Through research, education, workforce development, and technology transfer, we help create a connected world. MTI leads the Mineta Consortium for Equitable, Efficient, and Sustainable Transportation (MCEEST) funded by the U.S. Department of Transportation, the California State University Transportation Consortium (CSUTC) funded by the State of California through Senate Bill 1 and the Climate Change and Extreme Events Training and Research (CCEETR) Program funded by the Federal Railroad Administration. MTI focuses on three primary responsibilities:

Research

MTI conducts multi-disciplinary research focused on surface transportation that contributes to effective decision making. Research areas include: active transportation; planning and policy; security and counterterrorism; sustainable transportation and land use; transit and passenger rail; transportation engineering; transportation finance; transportation technology; and workforce and labor. MTI research publications undergo expert peer review to ensure the quality of the research.

Education and Workforce Development

To ensure the efficient movement of people and products, we must prepare a new cohort of transportation professionals who are ready to lead a more diverse, inclusive, and equitable transportation industry. To help achieve this, MTI sponsors a suite of workforce development and education opportunities. The Institute supports educational programs offered by the Lucas Graduate School of Business: a Master of Science in Transportation Management, plus graduate certificates that include High-Speed and Intercity Rail Management and Transportation Security Management. These flexible programs offer live online classes so that working transportation professionals can pursue an advanced degree regardless of their location.

Information and Technology Transfer

MTI utilizes a diverse array of dissemination methods and media to ensure research results reach those responsible for managing change. These methods include publication, seminars, workshops, websites, social media, webinars, and other technology transfer mechanisms. Additionally, MTI promotes the availability of completed research to professional organizations and works to integrate the research findings into the graduate education program. MTI's extensive collection of transportation-related publications is integrated into San José State University's world-class Martin Luther King, Jr. Library.

Report 24-44

Experimental Investigations of Wind Shear from Passing a Vehicle

Hamid Rahai, PhD

Assma Begum

Jeremy Bonifacio, PhD

Ryan Moffit

December 2024

A publication of the
Mineta Transportation Institute
Created by Congress in 1991

College of Business
San José State University
San José, CA 95192-0219

TECHNICAL REPORT DOCUMENTATION PAGE

1. Report No. 24-44	**2. Government Accession No.**	**3. Recipient's Catalog No.**	
4. Title and Subtitle Experimental Investigations of Wind Shear from Passing a Vehicle		**5. Report Date** December 2024	
		6. Performing Organization Code	
7. Authors Hamid Rahai, PhD ORCID: 0000-0003-4171-466X Assma Begum ORCID: 0009-0006-4388-9868 Jeremy Bonifacio, PhD ORCID: 0000-0002-8497-769X Ryan Moffit ORCID: 0009-0002-5665-9026		**8. Performing Organization Report** CA-MTI-2334	
9. Performing Organization Name and Address Mineta Transportation Institute College of Business San José State University San José, CA 95192-0219		**10. Work Unit No.**	
		11. Contract or Grant No. ZSB12017-SJAUX	
12. Sponsoring Agency Name and Address State of California SB1 2017/2018 Trustees of the California State University Sponsored Programs Administration 401 Golden Shore, 5th Floor Long Beach, CA 90802		**13. Type of Report and Period Covered**	
		14. Sponsoring Agency Code	
15. Supplemental Notes 10.31979/mti.2024.2334			

16. Abstract

Wind energy can be harnessed for various commercial and transportation-related applications. This study assessed experimentally the potential of capturing wind energy from the passage of vehicles for electric power generation. Both wind tunnel experiments and field tests were performed. The wind tunnel experiments were performed in an open-circuit low-speed wind tunnel at a free-stream mean velocity of 23 m/s. Five PVC pipes placed adjacent to the wind-blowing domain were used to simulate the columns under a freeway overpass. A scaled Ahmad body (simplified car body model) was used as the vehicle. The spanwise distance between the Ahmad body and the tubes was 0.75 W where W is the width of the vehicle. The middle tube was used as a reference tube for circumferential and vertical pressure measurements. The streamwise locations of the vehicle were according to our previous transient numerical simulations as the vehicle approached and passed the columns at 0.1–0.5 sec. Results showed a significant potential of the transient wind generated from passing vehicles and identified optimized locations for harnessing this wind for electric power generation. Field tests were performed using a moving scaled Ahmad body. The vehicle speed was approximately 22 miles/hr (10 m/s.). Wind measurements were made up to 0.75 W adjacent to a vertical wall with static and total pressure taps. Results verified the corresponding wind tunnel results and showed a maximum transient wind of 10 m/s from the passing of the vehicle. These results were in agreement with our previous simulation results. The experiment results suggest great potential for harnessing the wind from vehicles to generate electric power, benefiting California's renewable energy goals.

17. Key Words Wind power, Sustainability, Wind energy, Transportation technology, Energy harvesting.	**18. Distribution Statement** No restrictions. This document is available to the public through The National Technical Information Service, Springfield, VA 22161.		
19. Security Classif. (of this report) Unclassified	**20. Security Classif. (of this page)** Unclassified	**21. No. of Pages** 24	**22. Price**

Form DOT F 1700.7 (8-72)

DOI: 10.31979/mti.2024.2334

Mineta Transportation Institute
College of Business
San José State University
San José, CA 95192-0219

Tel: (408) 924-7560
Fax: (408) 924-7565
Email: mineta-institute@sjsu.edu

transweb.sjsu.edu/research/2334

ACKNOWLEDGMENTS

Funding for this research was provided by the California State University Transportation Consortium through the State of California's Senate Bill 1, the Road Repair and Accountability Act of 2017.

CONTENTS

LIST OF FIGURES

Executive Summary

We experimentally investigated the transient wind generated from the passing of a vehicle near a wall and a set of columns for potential electric power generation. Capturing this energy would add to California's renewable energy portfolio for various commercial and transportation-related applications. Our current experimental and past numerical investigations have shown that, in the context of freeway applications, where the frontal shape of the vehicle is the most effective in generating wind, a wind equivalent to the vehicle's speed is generated at a distance equivalent to the 50% width of the vehicle in the spanwise direction and maintains uniformity in a vertical spacing up to the top of the vehicle. Under freeway overpasses, near a wall or a column, the wind generated is contained and has a more uniform energy potential for electric power generation. With an optimized wind turbine system, this energy potential can be harnessed to generate electricity for lighting freeways for improved safety and powering signs and notification systems.

Our research and development over the past decades have resulted in a high-efficiency vertical-axis wind turbine system with a power coefficient of nearly 0.4 over a large range of tip-speed ratios. The wind turbine system comes with backup battery storage, a voltage regulator, and an optional inverter. It can be scaled to different sizes for different levels of power generation. Depending on the blade surface area and stacking and the type of generator used, the power output ranged from 100 watts to more than 2 kilowatts. With an appropriate adjustment to this system, we believe we will be able to develop an effective wind farm along the freeway for significant electric power generation.

1. Introduction

Experimental investigations [1] of the wind load generated by vehicles on road signs have shown that the force acting on these signs during the passage of a vehicle differs with respect to the aerodynamics of the vehicle and the location of the sign. The greatest force on the road sign is imposed by the front of the vehicle, and the amount of the load depends on the distance between the vehicle and the sign. Depending on the force's amplitude and its duration, the impact on the road sign could result in dynamic reactions and material fatigue.

Other investigations [2–9] on load-induced on-road signs and vehicle-induced gusts have provided similar results, though they include additional details of the wind profiles around vehicles. A study [10] on the effect of natural wind on road signs has shown a reduced mean drag coefficient as compared to the corresponding value published by the American Association of State Highway and Transportation with its variations depending on the aspect and depth ratios of the sign.

Recent unsteady numerical simulations of an Ahmed body under a freeway overpass [11, 12] have shown that when the vehicle is at a distance of 0.75 W from the bridge column, where W is the width of the vehicle, gusts of up to 23 meters per second (m/s), i.e., 51.5 miles per hour (mph) or 82.4 kilometers per hour (km/h), are generated near the bridge column. In this area, turbulent kinetic energy and vorticity are reduced indicating reduced fluctuations in the wind generated. On the top of the vehicle near the end, the wind speed is higher than 24 m/s, which decreases downstream. As the vehicle passes the columns, in the vehicle's wake, vortices are increased and expanded, and the turbulent kinetic energy is amplified.

The bridge's constraints cause changes in the baseline vehicle pressure which affects the transient vehicle's drag coefficient. The transient wind generated at the columns is mostly caused by the front of the vehicle and ranges from 6 m/s to 10 m/s. The circumferential pressure distributions on the referenced column show that the stagnation point changes with the passing of the vehicle with a maximum differential pressure coefficient of 0.2. The ground effects are seen up to 5 m elevations where the pressure coefficient changes from positive to negative with the passing of the vehicle, with a maximum difference of 0.17.

The present investigations are continuations of our previous numerical investigations [11, 12] which experimentally investigated the wind generated from passing vehicles near freeway walls and poles, with a goal of determining its potential for electric power generation.

2. Experimental Investigations

2.1 Wind Tunnel Experiments

The experiments were conducted in the Center for Energy and Environmental Research & Services's low-speed open-circuit wind tunnel which consists of six main components: the motor, blower, diffuser, settling chamber, contraction, and test section. Air is driven through the tunnel by a 3750 CFM backward airfoil centrifugal blower, powered by a 3 HP electric motor. The diffuser is a two-part diffuser expanding from 43.2 by 63.5 cm to 76.2 by 76.2 cm over a distance of 91.4 cm. Boundary layer control is provided by a screen with an open area ratio of 62.4% paced across the flow in the middle of the diffuser. The diffuser section is followed by the settling chamber which has a hexagonal honeycomb (3.8 cm deep with 3.2 mm cells) and three screens with open area ratios of 62.4%, 59.1%, and 59.1%, respectively. Following the settling chamber is a 3-D contraction with a 10:1 area ratio over a distance of 91 cm. From the contraction, the flow is passed through a two-dimensional diffuser to a cross-sectional area of 38.1 by 30.48 cm. The diffuser is followed by an open working area with a 1.27 cm thick polished wooden flat plate of 122 cm width and 244 cm length, which is aligned with the bottom surface of the diffuser. At the diffuser's outlet, in the range of 3 to 35 m/s, the mean velocity varies by less than 0.5%, and at all speeds; the background intensity is less than 0.2%.

The experiments were performed at a free-stream mean velocity of 23 m/s. Five PVC pipes with outer diameters of 6 cm and 90 cm long were placed on a flat plate platform adjacent to the wind-blowing domain in the streamwise direction at 2 diameters from each other. Figure 1 shows the experimental setup and the Ahmed body. The pipes simulate the columns under a freeway overpass. A scaled Ahmad body with dimensions of 17.36 cm height, 15.67 cm width, and 52.7 cm length was used as the vehicle.

Figure 1. The Ahmed Body and the Vertical Columns

The spanwise distance between the Ahmad body and the tubes was 0.75 w where w is the width of the vehicle. Previous numerical studies have shown that the 0.75 w distance is effective in generating high transient wind potential near freeway columns. The middle pipe was used as a

reference pipe for circumferential and vertical pressure measurements (Figure 2). Axial pressure taps were placed on the surface across the mid-section plane of the vehicle to investigate the change in vehicle pressure distribution and form drag due to flow constraints caused by the tubes. The static pressure taps had an inner diameter of 1 mm and an outer diameter of 2 mm. For the monitoring tube, there were 36 circumferential static pressure taps at 10-degree spacing, placed at half the height of the vehicle from the floor of the wind tunnel (Figure 2).

Figure 2. Circumferential Pressure Measurements and the Vehicle

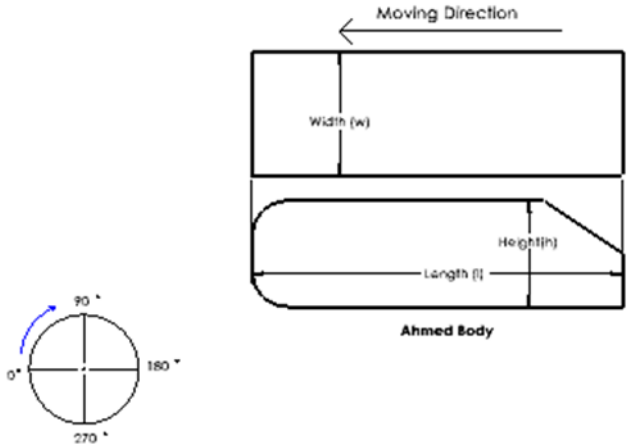

There were 13 vertical pressure taps at the 90-degree angle location. The first tap was at 0.058 h from the ground, where h is the height of Ahmed's body. The rest were spaced covering 1.82 h vertical distance (Figure 3).

Figure 3. Locations of Vertical and Circumferential Static Pressure Measurements

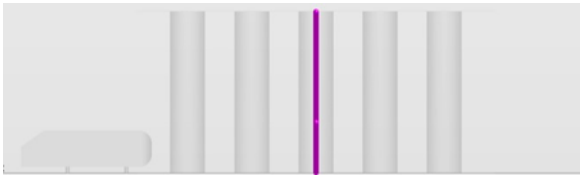

(a)

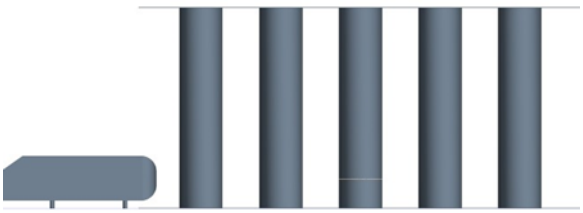

(b)

All pressure taps were connected to two 16-channel Scanivalve DSA 3200 and 5000 systems connected to a laptop computer. Two thousand and forty-eight samples were collected at a rate of 2,048 samples per second for each pressure tap and averaged for static pressure measurements. The streamwise locations of the vehicle were according to our previous transient numerical simulations as the vehicle approached and passed the columns at 0.1–0.5 seconds (Figure 4).

Figure 4. Vehicle Locations at Different Time Steps

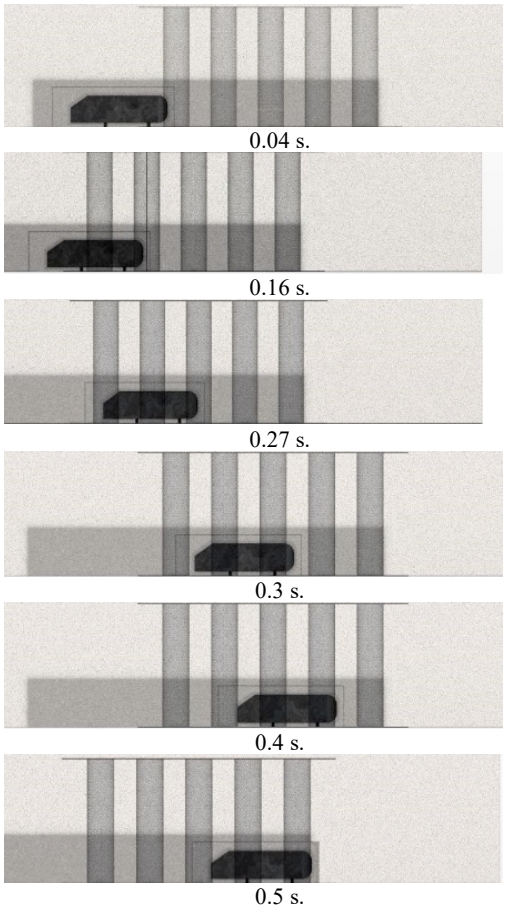

2.2 Field Tests

The field tests were conducted using a scaled model of the Ahmed body mounted on a radio-controlled car frame which is capable of moving the vehicle at up to 30 mph (Figure 5). The Ahmed body's dimensions were 35.6 cm in width, 30.48 cm in height, and 101.6 cm in length. The spacing between the ground and the vehicle was 2.86 cm.

Figure 5. The Field Test With the Ahmed Body

A wooden board of approximately 122 cm in width and 178 cm in length was used as the wall. The wall had axial and vertical pressure taps for monitoring static pressure from the passing vehicles. The pressure taps were stainless steel tubes of 1.34 mm outside diameter (O.D.) and 1.65 mm inside diameter (I.D.). The wall had eight horizontal static pressure taps at half the height of the vehicle. The first tap was 26 cm from the leading edge of the wall, and the following six taps were spaced evenly 15.24 cm apart. The last tap was placed 163.2 cm from the wall's leading edge. The vertical static pressure taps were 127 cm from the wall's leading edge. Five static pressure taps were used for vertical static pressure measurements. The taps were at 0.5 cm, 1.5 cm, 2 cm, 4 cm, and 8.5 cm from the ground, respectively. Three 90-degree total pressure tubes were also installed in the vertical direction at the same axial location as the vertical pressure taps at a spacing of 1 cm, 2.5 cm, and 5.5 cm, respectively, from the ground. They were installed to monitor wind velocity gradient in the vertical direction. The spacing between the tip of the probes and the wall was 2.54 cm.

An equilateral triangular aluminum rake with ten total pressure tubes measured wind velocity in the spanwise direction. Figure 6 shows the rake. The aluminum rake was 2.6 mm thick. The tubes were spaced such that they could measure total pressure without interference from the other tubes. The approximate spacing between the tubes was 1.4 cm and between the wall and the furthest tube was 13.41 cm.

Figure 6. Rake for Spanwise Velocity Measurements

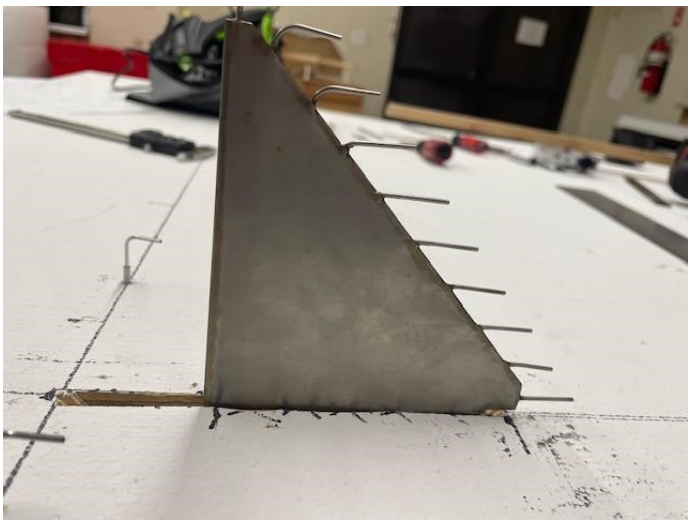

To maintain a distance of 0.75 w between Ahmed's body and the wall, the vehicle was attached to two arms with guide rails on the side of the vehicle. The guide rails were placed inside an aluminum rail that forced the vehicle to move in a straight line. The vehicle was placed approximately 10 m upstream of the wall and moved at a speed of 10 m/s. The speed was monitored by a handheld speed gun with an accuracy of 0.44 m/s.

The same Scanivalve systems were used to measure static and total pressure measurements. Transient pressure measurements were made at 2,048 samples/s.

3. Results and Discussions

3.1 Wind Tunnel Results

Figure 7 shows the variation of the circumferential pressure coefficient at different time steps corresponding to the locations of the front of the vehicle at the reference location. All pressure differential values have been normalized by the wind tunnel's dynamic pressure to obtain the pressure coefficients. At 0.1 second, the front of the vehicle is at -15.6 cm distance from the reference plane, and the corresponding distances at 0.2, 0.25, 0.265, 0.28, 0.29, 0.3, 0.4, and 0.5 seconds are -5.2, -2.5, -1.25, 0, 1.25, 2.5, 26.5, and 58 cm, respectively, where a negative distance indicates that the front of the vehicle has not passed the reference plane.

At 0.1 seconds, the pressure coefficient was 0.023 at 30 degrees, reduced to -0.13 at 160 and 180 degrees, and at other locations mostly fluctuated around zero. At this time, the location of the vehicle is far from the reference pipe and the flow movement around the reference pipe is limited.

Between 0.2–0.5 seconds, the maximum differences in pressure coefficient ranged between 0.08 at 0.2 seconds to higher than 0.1 at 0.3 seconds. At 0.29 seconds, the vehicle's leading edge was at the reference pipe, and at 0.3 seconds, it just passed the reference pipe, which indicates that the vehicle's leading edge is mostly responsible for the changes in the circumferential pressure and the gust generated at this location.

Figure 8 shows the variation of the vertical pressure coefficient at different time steps. The vertical distance Y was normalized by the height of the vehicle. To obtain the pressure coefficients, the vertical pressure differential values were normalized by the wind tunnel dynamic pressure. At 0.1 seconds, as the vehicle approaches the reference column, the vertical pressure fluctuates between zero and a minimum pressure of -0.3 at the mid-section plane and above the vehicle. The pressure fluctuations are reduced with the approaching of the vehicle and between 0.25 to 0.4 seconds, while the variations are similar to the corresponding variations at 0.1 seconds, but are reduced to a minimum pressure of -0.2. These variations correspond to the passage of the vehicle and the near wake area. At 0.5 seconds, the pressure coefficient approaches zero.

Reviewing the vertical pressure variations, it is noticeable that the pressure coefficients are negative between the ground and the top of the vehicle at all times, corresponding to air movements from the passing of the vehicle at these locations. This means that to extract wind energy from the passing of vehicles, the wind turbine system should be placed between the ground and the top of the vehicle.

Figure 7. Variations of the Circumferential Pressure Coefficient at Different Time Steps

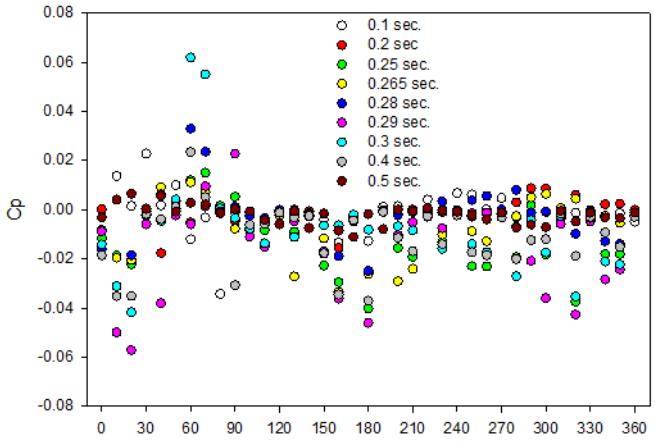

Figure 8. Variations of the Vertical Pressure Coefficient at Different Time Steps.

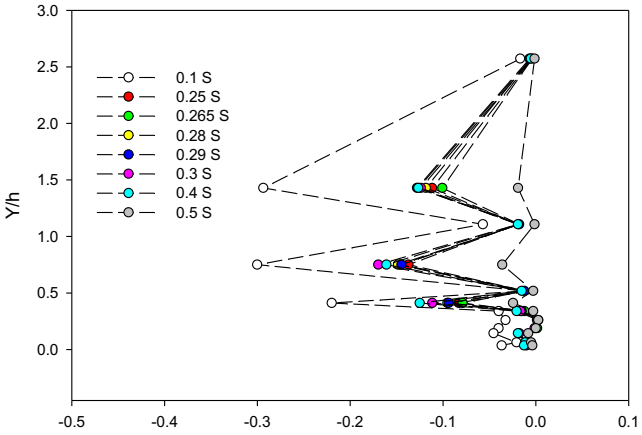

Figure 9 shows the variation of the axial pressure coefficient at the mid-section plane of the vehicle at different time steps. The results also include the pressure distribution for the vehicle without the poles for comparison. All pressure differentials have been normalized by the corresponding stagnation pressure differential to obtain the pressure coefficients. For all cases, the pressure drops to a minimum from the stagnation point due to fluid acceleration. The lower pressures are associated with time steps 0.28 and 0.3 when the vehicle's leading edge is near or at the reference pole location. The pressure drop is the lowest at the 0.1 second time step. The pressure coefficients then increase and become zero at X/L = 0.2, where X is the axial distance and L is the length of the vehicle. Between X/L = 0.0 and 0.2, for time steps 0.28 and 0.5, there are decreases and increases in pressure. The pressure remains zero in all other cases. Between X/L = 0.6 and 0.8, the pressure coefficient is zero in all cases.

The pressure coefficient decreases at X/L = 0.8, which corresponds to the start of the slanted surface near the back of the Ahmed body. The slant is at 30 degrees in the clockwise direction and terminates at the back of the vehicle. This location is the start of flow separation. The lowest

pressures are at X/L = 0.85, and the least pressure is exerted at the 0.3 second time step. The pressure coefficients increase thereafter and approach zero at the back of the vehicle.

Compared with the pressure distribution of the vehicle without the poles, the presence of the poles causes changes in the flow conditions across the vehicle when the vehicle approaches and passes the poles, resulting in a slight increase in the vehicle's drag coefficient.

Figure 9. Variation of the Pressure Coefficient Across the Axial Mid-Section of the Vehicle

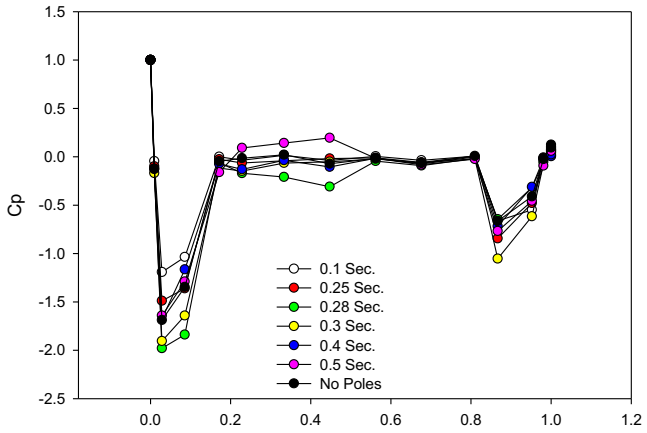

3.2 Field Tests

Figure 10 shows variations of the transient axial pressure coefficient caused by the passage of the vehicle at different axial locations. The static pressure differentials with the moving vehicle have been divided by the corresponding values without the vehicle in place to obtain the pressure coefficients. The leading edge of the vehicle reaches the first static pressure tap at approximately 0.45 seconds with a peak Cp of 0.2 followed by a drop in pressure coefficient to less than -0.2 before recovering to a value less than 0.2 at about 0.455 seconds. The pressure coefficient drops again to an approximate value of -0.3 before it increases again and approaches zero at 0.457 seconds. These variations correspond to the passage of the vehicle with positive pressure corresponding to the leading edge and immediate tail of the vehicle and negative pressures corresponding to the passage of the body and the wake area. The total difference in pressure coefficients is approximately 0.5. Similar variations in the pressure coefficient are seen for other horizontal pressure taps with delayed times.

Figure 11 shows transient variations of the vertical pressure coefficient at different vertical locations. When the vehicle passes the reference column, for all pressure taps, the pressure coefficient peaks at 0.2 before it drops to -0.6, then it increases again to a Cp of 0.2, before it drops again, but remains on the positive side. Between 4.35% to 11.6% of the vehicle's height, the pressure coefficient shows an additional peak of higher than 0.2, before it decreases and approaches zero. The passage of the vehicle changes the vertical pressure coefficient with a maximum difference of slightly higher than 0.8. Beyond 24.6% of the vehicle's height, we did not observe

much difference in the vertical static pressure coefficient which means the ground effect has disappeared at elevations beyond 25% of the vehicle's height.

Figure 12 shows the spanwise variation of the mean velocity U from the passing of the vehicle calculated from the rake pressure measurements. Here Z is the spanwise distance normalized by the width of the vehicle. There is an approximate linear increase in the mean velocity with increased distance from the wall and at approximately 50% of the width of the vehicle, the mean velocity is higher than 12 m/s, which is higher than the speed of the vehicle. These results show that the wind energy potential is high at the mid-section height of the vehicle and at about 50% of the vehicle's width, with a maximum static pressure coefficient of 0.8.

Figure 10. Transient Axial Pressure Coefficient

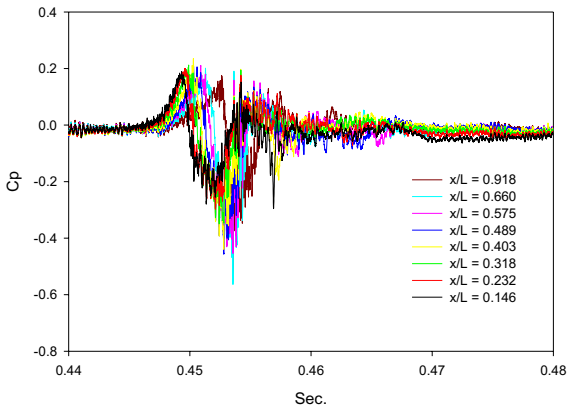

Figure 11. Transient Vertical Pressure Coefficient

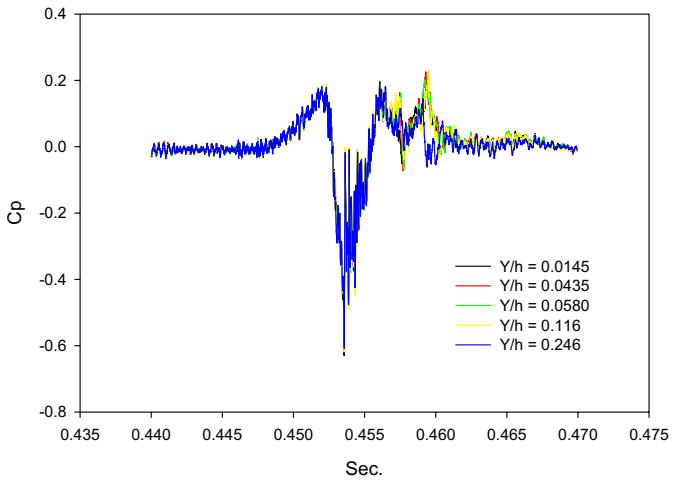

Figure 12. Spanwise Velocity from Passing of the Vehicle

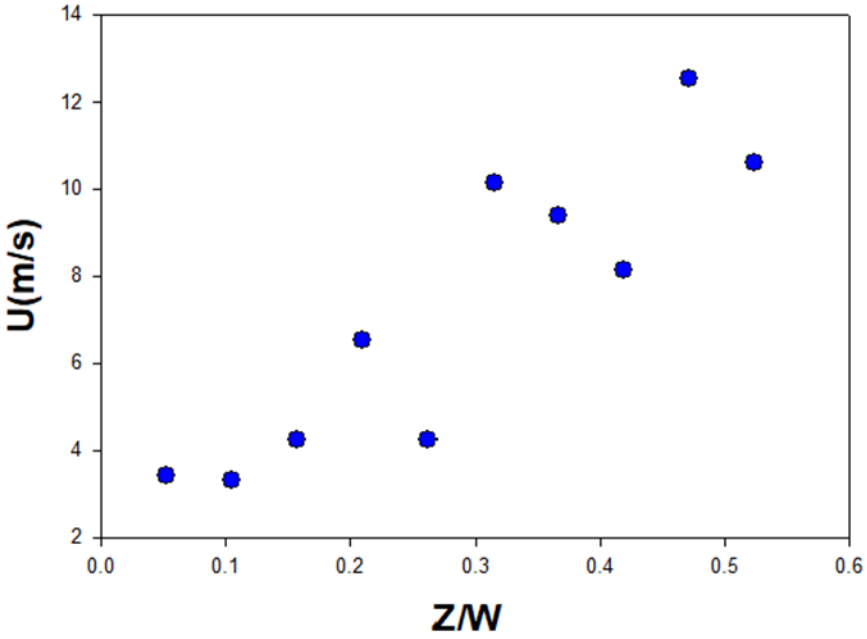

4. Summary & Conclusions

The goal of the investigations was to experimentally investigate the wind energy potential from the passage of a vehicle and compare the results with corresponding numerical results to identify an optimum location for generating electricity. The study used a scaled Ahmad body for both wind tunnel measurements and field tests. Results confirmed our previous numerical investigations of the existence of significant wind energy potential from the passage of vehicles on freeways and highways. The maximum wind gust generated was equivalent to the speed of the vehicle up to 0.5 w spanwise distance from the vehicle. At this location, the wind speed was sustained in the vertical direction from above the ground to the top of the vehicle. These results agree with our previous numerical simulations using a scaled Ahmed body traveling at 23 m/s on a California freeway.

Endnotes

1. Lichtneger, P., and B. Ruck. "Full-Scale Experiments on Vehicle Induced Transient Loads on Roadside Plates." *J. Wind Eng. Ind. Aerodyn.* 136 (2015): 73–81.

2. Ruck, B., and P. Lichtneger. "Wind Loads on Flat Board and Walls Induced by Passing." *Fachtagung: Lasermethodyn in der Strömungsmesstechnik* (September 2014). https://gala-ev.org/images/Beitraege/Beitraege%202014/pdf/14.pdf

3. Salvadori, S., Morbiato, T., Mathana, A., and E. Fusto. "On the Characterization of Wind Profile Generated by Road Traffic." In *Seventh International Colloquium on Bluff Body Aerodynamics and Applications (BBAA7)*, 1729–1741. Shanghai, China: September 2012.

4. Sanz-Andres, A., Santiago-Prowald, J., Baker, C., and A. Quinn. "Vehicle-Induced Loads on Pedestrian Barriers." *J. Wind Eng. Ind. Aerodyn.* 92 (2003): 413–426.

5. Sanz-Andres, A., Laveron, A., and A. Quinn. "Vehicle-Induced Loads on Traffic Sign Panels." *J. Wind Eng. Ind. Aerodyn.* 91 (2003): 925–942.

6. Quinn, A. D., Baker, C. J., and N. G. Wright. "Wind and Vehicle Induced Forces on Flat Plates- Part I: Wind Induced Forces." *J. Wind Eng. Ind. Aerodyn.* 89 (2001): 811–823.

7. Quinn, A. D., Baker, C. J., and N. G. Wright. "Wind and Vehicle Induced Forces on Flat Plates- Part II: Vehicle Induced Forces." *J. Wind Eng. Ind. Aerodyn.* 89 (2001): 831–847.

8. Cali, P. M., and E. E. Covert. "Experimental Measurements of the Loads Induced on an Overhead Highway Sign Structure by Vehicle-Induced Gusts." *J. Wind Eng. Ind. Aerodyn.* 84 (2000): 87–100.

9. Zou, Y., Fu, Z., He, X., Cai, C., Zhou, J., and S. Zhou. "Wind Load Characteristics of Wind Barriers Induced by High-Speed Trains Based on Field Measurements." *Appl. Sci.* 9 (2019), 4865. doi:10.3390/app9224865.

10. Meyer, D., Zisis, I., Hajra, B., Chawdhury, A. G., and P. Irwin. "An Experimental Study on the Wind-Induced Response of Variable Message Signs." *Frontiers in Build Environment* Vol. 3 (2017), Article 66.

11. Rahai, H., and A. Begum. "Numerical Investigations of Transient Wind Shear from Passing Vehicles near a Road Structure." *SAE Technical Paper* 2021-01-0964. doi:10.4271/2021-01-0964.

12. Rahai, H., and A. Begum. "Large Eddy Simulations of Wind Shear from Passing Vehicles Under a Freeway Overpass." APS DFD 76th Annual Meeting, Nov. 19–21, Washington DC, 2023.

About the Authors

Hamid Rahai, PhD

Dr. Hamid Rahai is a professor in the Department of Mechanical and Aerospace Engineering & Biomedical Engineering and is the director of the Center for Energy and Environmental Research & Services (CEERS) in the College of Engineering at California State University, Long Beach (CSULB). He has taught various classes at the undergraduate and graduate levels in thermal sciences, supervised over 70 M.S. theses and projects and Ph.D. dissertations, and published more than 100 technical papers. He has been granted patents for the development of a high-efficiency vertical axis wind turbine (VAWT) and wind turbine apparatuses and for reducing NOx emission of Cargo Handling Equipment using a Humid Air System. He also has pending patents related to an environmental artificial tree designed to reduce ambient NOx and a new guide-vane enclosure for capturing wind energy from passing vehicles. Dr. Rahai is the recipient of the 2004 Northrop Grumman Excellence in Teaching Award and the 2012 CSULB Impact Accomplishment of the Year in RSCA Award. He received the Outstanding Engineering Educator Award from the Orange County Engineering Council in California in 2014, and in 2019 he was inducted as a senior member of the National Academy of Inventors (NAI).

Assma Begum

Ms. Assma Begum is a graduate student in the joint PhD program between the CSULB College of Engineering and the Claremont Graduate University (CGU) and a research assistant at the Center for Energy and Environmental Research & Services (CEERS) in the College of Engineering at CSULB. She has been involved in various projects at CEERS related to the aerodynamics of rotating cylinders and wind shears from passing vehicles and is author and co-author of two technical conference papers and one journal paper.

Jeremy Bonifacio, PhD

Dr. Jeremy Bonifacio is a teaching professor and a senior researcher at the CEERS in the College of Engineering at CSULB. His expertise is experimental and computational fluid mechanics. He has been involved in various applied industrial projects at CEERS and is co-owner of several patents related to emission control technologies and the application of CFD in diagnosing lung diseases. Dr. Bonifacio is the winner of the CSULB 2014 innovation challenge.

Ryan Moffit

Mr. Ryan Moffit is a graduate student in the joint PhD program between CSULB's College of Engineering and CGU and a research assistant at the Center for Energy and Environmental Research & Services (CEERS) in the College of Engineering at CSULB. Mr. Moffit is an experimentalist. His research is focused on finding an optimized surface geometry for reducing the drag of vehicles. He has authored and co-authored two ASME conference papers.

MTI FOUNDER

Hon. Norman Y. Mineta

MTI BOARD OF TRUSTEES

Directors

MTI MINETA TRANSPORTATION INSTITUTE